Biochemical Pharmacology 78 (2009) 583–591

Contents lists available at ScienceDirect

Biochemical Pharmacology

journal homepage: www.elsevier.com/locate/biochempharm

Inhibition of ATP synthase by chlorinated adenosine analogue

Lisa S. Chen [a], Billie J. Nowak [a], Mary L. Ayres [a], Nancy L. Krett [b], Steven T. Rosen [b], Shuxing Zhang [a,1,*], Varsha Gandhi [a,c,1,*]

[a] Department of Experimental Therapeutics, University of Texas M. D. Anderson Cancer Center, Houston, TX 77030, USA
[b] Robert H. Lurie Comprehensive Cancer Center, Northwestern University, Chicago, IL 60611, USA
[c] Department of Leukemia, University of Texas M. D. Anderson Cancer Center, Houston, TX 77030, USA

ARTICLE INFO

Article history:
Received 20 March 2009
Accepted 18 May 2009

Keywords:
ATP synthase
8-Chloroadenosine
Cellular bioenergy
Molecular modeling
Nucleoside analogue
Chemotherapeutics

ABSTRACT

8-Chloroadenosine (8-Cl-Ado) is a ribonucleoside analogue that is currently in clinical trial for chronic lymphocytic leukemia. Based on the decline in cellular ATP pool following 8-Cl-Ado treatment, we hypothesized that 8-Cl-ADP and 8-Cl-ATP may interfere with ATP synthase, a key enzyme in ATP production. Mitochondrial ATP synthase is composed of two major parts; F_O intermembrane base and F1 domain, containing α and β subunits. Crystal structures of both α and β subunits that bind to the substrate, ADP, are known in tight binding ($\alpha_{dp}\beta_{dp}$) and loose binding ($\alpha_{tp}\beta_{tp}$) states. Molecular docking demonstrated that 8-Cl-ADP/8-Cl-ATP occupied similar binding modes as ADP/ATP in the tight and loose binding sites of ATP synthase, respectively, suggesting that the chlorinated nucleotide metabolites may be functional substrates and inhibitors of the enzyme. The computational predictions were consistent with our whole cell biochemical results. Oligomycin, an established pharmacological inhibitor of ATP synthase, decreased both ATP and 8-Cl-ATP formation from exogenous substrates, however, did not affect pyrimidine nucleoside analogue triphosphate accumulation. Synthesis of ATP from ADP was inhibited in cells loaded with 8-Cl-ATP. These biochemical studies are in consent with the computational modeling; in the $\alpha_{tp}\beta_{tp}$ state 8-Cl-ATP occupies similar binding as ANP, a non-hydrolyzable ATP mimic that is a known inhibitor. Similarly, in the substrate binding site ($\alpha_{dp}\beta_{dp}$) 8-Cl-ATP occupies a similar position as ATP mimic ADP-BeF_3^-. Collectively, our current work suggests that 8-Cl-ADP may serve as a substrate and the 8-Cl-ATP may be an inhibitor of ATP synthase.

1. Introduction

The nucleoside analogues currently used in the clinic are largely DNA-directed and act by inhibiting DNA synthesis [1]. These analogues either incorporate into DNA and/or affect metabolic enzymes such as ribonucleotide reductase [2], purine nucleoside phosphorylase [3], and adenosine deaminase [4,5] to perturb intracellular deoxynucleotide pools, resulting in decreased DNA synthesis in cells. In contrast, 8-chloroadenosine (8-Cl-Ado) contains a ribose sugar and is unique because it is RNA-directed. The advantage of RNA-directed agents such as 8-Cl-Ado is that they provide a valuable strategy for targeting quiescent cancers that do not actively synthesize DNA. Two RAID (Rapid Access to Interventional Development) contracts were awarded by the National Cancer Institute for the development of 8-Cl-Ado, and the drug is being tested in the first Phase I clinical trial for the treatment of chronic lymphocytic leukemia (CLL), an indolent leukemia. Ultimately, this agent will be used for other quiescent malignancies such as multiple myeloma and solid tumors.

In preclinical pharmacological studies using multiple myeloma (MM) cell lines and primary leukemia cells, 8-Cl-Ado was demonstrated to be phosphorylated into its triphosphate form (8-Cl-ATP) [6], which inhibits transcript synthesis by incorporation into RNA [7] and by inhibition of polyadenylation [8]. In addition, a decline in intracellular ATP is observed in cells treated with 8-Cl-Ado, however, by unknown mechanisms. Studies using cell lines that are proficient or deficient in adenosine kinase and in vitro kinase assays demonstrated that 8-Cl-Ado is monophosphorylated (8-Cl-AMP) by adenosine kinase [6,9]. 8-Cl-AMP is further metabolized to 8-Cl-ADP and 8-Cl-ATP, which are presumed to be catalyzed by monophospho-kinase and diphospho-kinase, respectively. We previously demonstrated that 8-Cl-ATP accumulates at high levels (>400 μM) [6,10] while ATP levels decline to 50% of control after 6 h of treatment. The endogenous ATP concentration was reduced from ~1.7 mM to 0.65 mM a 12-h

* Corresponding authors at: Department of Experimental Therapeutics, Unit 71, UT M. D. Anderson Cancer Center, 1515 Holcombe Blvd., Houston, TX 77030, United States. Tel.: +1 713 792 2989; fax: +1 713 794 4316.
E-mail addresses: shuzhang@mdanderson.org (S. Zhang), vgandhi@mdanderson.org (V. Gandhi).
[1] These authors contributed equally to this work.

0006-2952/$ – see front matter © 2009 Elsevier Inc. All rights reserved.
doi:10.1016/j.bcp.2009.05.019

incubation with 8-Cl-Ado in cell lines, and similar phenomenon was observed in primary leukemia cells obtained from the peripheral blood of patients with CLL [10].

The majority of cellular ATP is synthesized using respiratory chain oxidative phosphorylation by ATP synthase, which is the last enzyme in the respiratory chain [11]. ATP synthase catalyzes the synthesis of ATP from recycling ADP [12–15], and it has been associated with a number of human diseases including cancer (for a review, see [16]). Studies suggest that cell surface ATP synthase can function as a receptor for ligands involved in several cellular processes including regulation of cell proliferation and differentiation, and immunological tumor recognition [17,18]. Elevated expression of ATP synthase on endothelial cell surfaces has been reported to play an important role during angiogenesis, and angiostatin action is in part via the inhibition of cell surface ATP synthase [19]. As such, recent developments have highlighted ATP synthase as a potential cancer target for therapeutics. Aurovertin B, an ATP synthase inhibitor, is currently under investigation for the treatment of breast cancer and has been shown to inhibit proliferation and induce apoptosis [20]. More recently, monoclonal antibodies against ATP synthase was reported to inhibit proliferation and colony formation in human vascular endothelial cells and reduce tumor growth in xenograft models [21,22].

In order to understand the function and mechanism of ATP synthase, X-ray crystal structures of both F_O and F1 domains have been obtained by others [12–15,23]. ATP synthase is composed of two major parts: the F_O domain, an intermembrane proton channel, and the F1 domain, the catalytic complex. The nucleotide binding/catalytic sites are within F1 domain, which is composed of five different subunits with stoichiometry $\alpha 3\beta 3\gamma\delta\varepsilon$. The crystal structures demonstrate that α and β subunits are structurally similar, and each subunit consists of three domains: a small N-terminal domain, a nucleotide binding domain and a helical C-terminal domain [12,13,23]. Both α and β subunits bind nucleotides but only the β subunit participates in the catalysis. It has been found that the three catalytic sites in the three β subunits have different affinities for nucleotides, and these together with other results have been used to propose a binding change mechanism of β units during the catalytic cycle of the enzyme [12–15]. It was proposed that rotation of the central F_O stalk interconverted the three binding sites of F_1 domain from open (low affinity binding) to tight (high affinity binding), from tight to loose (intermediate affinity binding), and from loose to open [23,24]. The structures of the F1-ATPase provided insight into the binding change mechanism: the different conformations of β-subunits account for the conformations proposed to occur during the catalytic cycle [12,13,23].

We hypothesized that 8-Cl-ADP may serve as a substrate of ATP synthase and that 8-Cl-ATP may be an inhibitor to this key enzyme based on the following prior observations. First, the structural similarities between Ado and 8-Cl-Ado or ATP and 8-Cl-ATP. Second, the use of 8-Cl-Ado or 8-Cl-ATP by the same enzymes as Ado and ATP, and third, a decline in cellular ATP pool after incubation of cells with 8-Cl-Ado. Using biological, biochemical, and computational molecular modeling studies our current work tested this hypothesis.

2. Materials and methods

2.1. Cell lines

All experiments were conducted using an exponentially growing multiple myeloma cell line, MM.1S [25,26]. All cells were routinely tested for *Mycoplasma* infection using a commercially available kit (Invitrogen, Carlsbad, CA).

2.2. Drugs and other chemicals

8-Cl-Ado was purchased initially from BioLog (La Jolla, CA) and then obtained from Dr. V. Rao at the Drug Development Branch of the NCI. [^{3}H]8-Cl-Ado and [^{3}H]Ado were purchased from Moravek Biochemicals (Brea, CA). 8-Cl-ATP was custom-synthesized by BioLog. Oligomycin was purchased from Sigma-Aldrich (St. Louis, MO). Coformycin (CF) and deoxycoformycin (dCF) were obtained from Dr. Robert Schultz at the NCI (Bethesda, MD). All other chemicals were reagent grade.

2.3. Oxygen consumption assay

Oxygen consumption is measured using a Hansatech Oxytherm (Hansatech Instrument, England). Drug treated cells are placed in sealed respiration chamber containing 1 mL of fresh culture medium pre-equilibrated with 21% oxygen. The sample temperature was regulated with a thermostat control and stirred with a micro-stirrer [27,28]. Oxygen levels were measured polarographically using a Hansatech oxygen electrode disc and the manufacturer's software.

2.4. Accumulation of Ado and 8-Cl-Ado metabolites

To quantitate the phosphorylated metabolites of Ado and 8-Cl-Ado, MM cells were incubated with oligomycin (2 μg/mL) for 30 min and then 10 μM [^{3}H]Ado or [^{3}H]8-Cl-Ado was added. The adenosine deaminase inhibitors CF and dCF (0.1 μM) were added to prevent deamination. The cellular nucleotides were extracted using the perchloric acid extraction procedure [6] and analyzed on a gradient that separates free nucleoside, mono-, di-, and triphosphate forms [29].

2.5. Measurement of intracellular nucleoside mono-, di-, and triphosphates by HPLC

For non-radioactive material, the cellular extracts were applied to an anion-exchange Partisil-10 SAX column as described before [6]. The column eluate was monitored by UV absorption at 256 nm, and 8-Cl-ATP was identified by comparing its retention profile and absorption spectrum with those of an authentic standard. The intracellular concentration of nucleotides contained in the extract was calculated from a given number of cells of a determined mean volume. The cell number was determined using Coulter counter (Coulter Electronics, Hialeah, FL). This equipment is attached to a channelizer which was used to estimate the mean volume of cells in a given cell population. This volume was used to quantitate the concentration of nucleotides. The lower limit of sensitivity of this assay was 10 pmol in an extract of 5×10^6 cells corresponding to a cellular concentration of 1 μM. For radioactive 8-Cl-Ado a Radiomatic Flow-through HPLC system (Packard, Downers Grove, IL) was used. The eluate from the anion-exchange column passed through an automatic radiometric detector along with liquid scintillation fluid (Ultima Flo, Packard) and tritium counts were recorded for each radioactive peak.

2.6. ATP synthase molecular docking studies

The ATP synthase structures (1BMF [23] and 2CK3 [24]) were obtained from Protein Data Bank (PDB [30]). In these crystal structures, ADP and ANP (an non-hydrolyzable ATP analogue) were observed at the interfaces of tight binding subunits ($\alpha_{dp}\beta_{dp}$) and loose binding subunits ($\alpha_{tp}\beta_{tp}$), respectively [23,24]. As such, both subunits from 1BMF were extracted to conduct the modeling studies. ADP and 8-Cl-ADP were docked into the catalytic site between $\alpha_{dp}\beta_{dp}$ while $\alpha_{tp}\beta_{tp}$ was used to probe its interactions

with ATP/8-Cl-ATP. In order to study the possible inhibitory effect on the enzyme, 8-Cl-ATP was also docked into the $\alpha_{dp}\beta_{dp}$ subunit of 2CK3 in which ADP-BeF_3^-, an analogue of ATP, showed inhibition to ATP synthase [24]. ADP and ANP were extracted from the crystal structure of 1BMF, followed with the correction of their chemical structures and the addition of all hydrogens. Since there is no crystal structure of the protein complexed with 8-Cl-ADP or 8-Cl-ATP, these two chemical structures were built based on the crystal structures of ADP and ANP, respectively. The structures were then used as our starting conformations in the docking process. Hydrogens were loaded to the complexes and all of the lone pairs were subjected to removal from both the ligands (ADP/8-Cl-ADP and ANP/ATP/8-Cl-ATP) and the receptors. Two docking packages, GOLD 3.2 [31] and AutoDock 3.0 [32], were employed to dock the ligands into the receptor catalytic sites. For the docking process a box with a dimension of 20 Å × 20 Å × 20 Å was created, centered at the geometrical center of the original ADP or ANP molecules accordingly. For the $\alpha_{dp}\beta_{dp}$ subunit of 2CK3, the geometrical center of ADP-BeF_3^- was utilized for modeling. During docking, the receptors were treated as rigid bodies while the ligands were flexible, and Mg^{2+}metal ion was kept in all docking as part of the binding pocket. All water molecules were removed from the receptors except for those in the $\alpha_{dp}\beta_{dp}$ subunit of 2CK3 in which a structural water molecule was maintained. All structures were prepared using MOE (Chemical Computing Group, Montreal, Quebec, Canada) [33], and all figures were created using PyMol (DeLano Scientific LLC, Palo Alto, CA) [34].

2.7. Statistical analysis

All statistical analyses were performed using GraphPad Prism software (GraphPad Software, Inc. San Diego, CA). Values of $p \leq 0.05$ were considered as statistically significant.

3. Results

3.1. 8-Cl-Ado and Ado incubation results in similar cellular O_2 consumption

The majority of ATP in cells is synthesized through oxidative phosphorylation that involves the mitochondrial respiration chain, which consists of complexes I–V [11]. To determine whether 8-Cl-Ado affects complexes I–IV, we compared O_2 consumption in whole cells when cells were treated with either Ado or 8-Cl-Ado. As expected, there was a change in O_2 consumption when cells were incubated with Ado or 8-Cl-Ado compared to control cells (Fig. 1A and B). However the change was not different between the two substrates Ado (Fig. 1 A) and 8-Cl-Ado (Fig. 1B).

3.2. Accumulation of 8-Cl-ATP and role of ATP synthase

To determine the role of ATP synthase in the accumulation of 8-Cl-ATP, oligomycin was used to inhibit the activity of this enzyme. When cells were treated with Ado, the accumulation of [^{3}H]ATP was 200, 400, and 1900 μM at 0.5, 1 and 3 h, respectively (Fig. 2A). When cells were pretreated with oligomycin prior to addition of [^{3}H]Ado, there was a decrease in formation of [^{3}H]ATP at all time points tested. Generally the decrease was about 50% of the control cells ($p = 0.012$, Fig. 2A).

3.3. Accumulation of 8-Cl-ATP and role of glycolysis

There have been numerous studies on the Warburg effect, examining the phenomenon that tumor cells have a high glycolysis rate, which is responsible for the generation of ATP. To establish the possible contribution of glycolysis in the formation of ATP or 8-Cl-ATP, we employed the use of deoxyglucose (dGlu), an inhibitor of glycolysis. Even using high levels of dGlu (10 mM), cells treated with dGlu still accumulated ~80% of ATP and 8-Cl-ATP levels of untreated cells (Supplemental Fig. 1), suggesting that ATP synthase is driving ATP source in our system. As expected, pretreatment of cells with both dGlu and oligomycin resulted in 80% decline in ATP or 8-Cl-ATP accumulation, however with these treatments, cells were undergoing apoptosis.

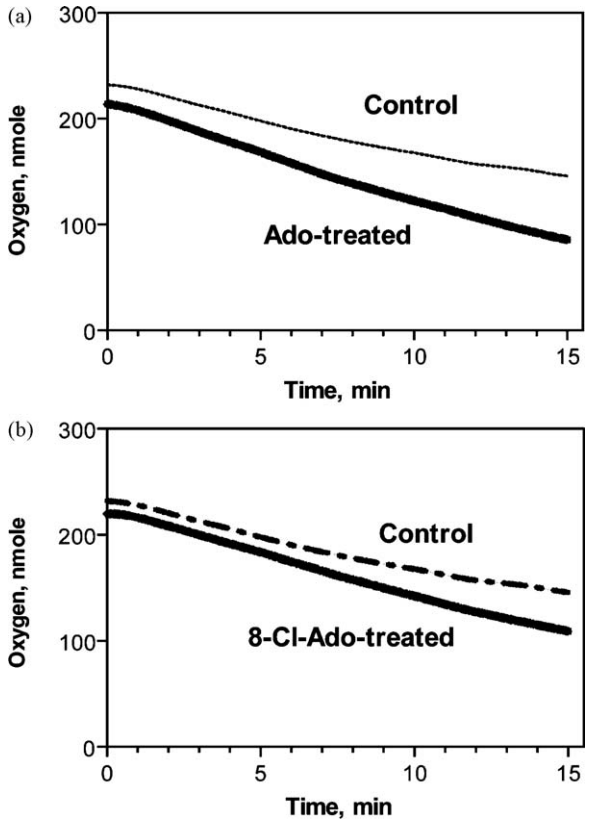

Fig. 1. 8-Cl-Ado does not affect O_2 consumption. MM.1S cells were incubated with either no drug (control), Ado (A) or 8-Cl-Ado (B), and O_2 consumption was measured using a respirometer. The experiments were performed in triplicate with similar results.

Treatment of cells with [^{3}H]8-Cl-Ado resulted in 150–170 μM [^{3}H]8-Cl-ATP at 0.5 h. This concentration remained fairly similar at 1 and 3 h (Fig. 2B). Hence, compared to ATP accumulation from [^{3}H]Ado, 8-Cl-ATP concentrations were 10-times lower. However, as observed in the oligomycin and Ado incubated cells, [^{3}H]8-Cl-ATP accumulation was also declined. The decrease was about 65% at all three time points ($p = 0.001$, Fig. 2B). Similar to 8-Cl-Ado, incubation with 8-Cl-cAMP (which serves as a precursor to 8-Cl-Ado [6]) also resulted in a 50% decrease in 8-Cl-ATP after treatment with oligomycin ($p = 0.042$, Fig. 2C).

To further determine if the inhibition of phosphorylation of [^{3}H]Ado and [^{3}H]8-Cl-Ado by oligomycin was only at the triphosphate level, we measured accumulation of the monophosphate, diphosphate, and triphosphates of Ado or 8-Cl-Ado. As shown in Fig. 2D, the primary decrease was in triphosphate formation. [^{3}H]ATP formation was decreased by 50% while [^{3}H]8-Cl-ATP accumulation was declined by 60% of control cells. Monophosphate or diphosphate remained either similar or slightly increased in cells treated with oligomycin (Fig. 2D).

In contrast to a decrease in triphosphate formation from 8-Cl-Ado or 8-Cl-cAMP after treatment of cells with oligomycin, accumulation of arabinosylcytosine triphosphate was not reduced when untreated or oligomycin-treated cells were incubated with

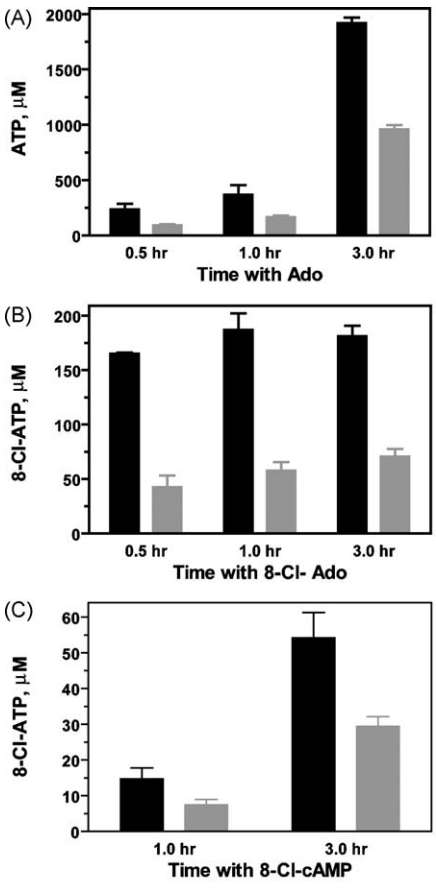

(D)

		[^{3}H] metabolite concentration (μM)		
		MP	DP	TP
[^{3}H] Ado	control	48 ± 11	236 ± 9	1919 ± 51
	oligomycin	77 ± 18	337 ± 9	960 ± 37
[^{3}H] 8-Cl-Ado	control	122 ± 2	34 ± 2	181 ± 10
	oligomycin	134 ± 10	35 ± 3	71 ± 7

Fig. 2. Inhibition of ATP synthase decreases ATP and 8-Cl-ATP accumulation but not monophosphate (MP) or diphosphate (DP) accumulation. MM.1S cells were pretreated with no drug (black bars) or 2 μg/mL oligomycin (a pharmacological inhibitor of ATP synthase, gray bars) for 30 min, then either [^{3}H]Ado (A and D), [^{3}H]8-Cl-Ado (B and D) or [^{3}H]8-Cl-cAMP (C) was added to the cells for indicated times or for 3 h (D). Accumulation of [^{3}H]AMP, [^{3}H]ADP, and [^{3}H]ATP or [^{3}H]8-Cl-AMP, [^{3}H]8-Cl-ADP, and [^{3}H]8-Cl-ATP was measured as described and are reported as ±SEM. At the end of incubations, the endogenous ATP pool in untreated cells was 2600 μM; in oligomycin alone, 8-Cl-Ado alone, and oligomycin + Ado treated cells was between 2350 and 2400 μM; in oligomycin + 8-Cl-Ado-treated cells it was 1960 μM; and 2800 μM in Ado treated cells. The results obtained were statistically significant ($p < 0.05$).

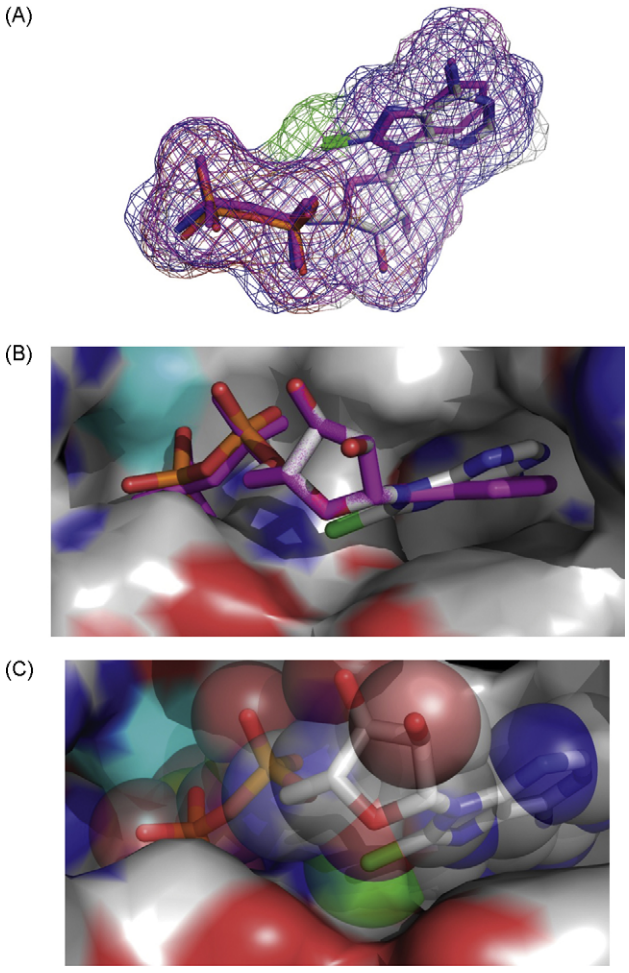

Fig. 3. Docking of 8-Cl-ADP into ATP synthase. (A) The docked 8-Cl-ADP by GOLD and AutoDock, and the crystal ADP structure. GOLD docked structure is colored based on atom types and AutoDock docked structure is in blue. Crystal ADP is shown in magenta, and the chlorine group is shown in green. The surfaces are in the net representation. (B) The surface analysis of the catalytic binding pocket, revealing a concave region to accommodate the –Cl group (green). Mg^{2+} (shown in cyan) forms charge-charge interactions with the diphosphate group. The color coded surface based on atom types is for the receptor binding pocket. The docked 8-Cl-ADP (from GOLD) is displayed in stick model (atom type-based color) and ADP is shown in magenta. For 3C, 8-Cl-ADP is in stick and transparent sphere display. complementarity instead of clash was observed between –Cl (green sphere) and the pocket surface, leading to stable binding of 8-Cl-ADP. This is due to the concave region mentioned above and the tilting of the adenine purine ring.

arabinosylcytosine (Supplemental Fig. 2). These data suggest that oligomycin treatment specifically affected ADP to ATP or 8-Cl-ADP to 8-Cl-ATP formation.

3.4. Molecular modeling with 8-Cl-ADP and ATP synthase

To determine whether 8-Cl-ADP is a substrate for ATP synthase, first we docked ADP into the binding site of the ATP synthase (1BMF) with GOLD and AutoDock. Both programs obtained the best docked poses with root mean square distance (RMSD) of 0.31 Å and 0.75 Å, respectively. With 8-Cl-ADP, these values were 0.43 Å by GOLD and 0.72 Å by AutoDock. Comparison between docked 8-Cl-ADP and crystal ADP revealed that the binding modes were similar except a small shift of the whole molecule (Fig. 3A). Most portions of the structure were well superimposed; in particular the sugar moiety was almost completely overlapped (with RMSD 0.03 Å), and there was only a very small deviation along the diphosphate group. The most obvious difference was observed around the adenine group: the angle between 8-Cl-ADP and ADP purine rings was about 22.60°, and there was a big bump on the surface of 8-Cl-ADP (Fig. 3A). Initial inspection of the binding pocket demonstrated that along the direction of hydrogen at C8-position on adenine, there existed a concave region which provided enough space to accommodate –Cl group (Fig. 3B). As further indicated in Fig. 3C, the –Cl surface indeed protruded into the small concave region and its volume just fitted in the space.

Detailed distance analysis of the starting conformation of 8-Cl-ADP (built from the ADP crystal structure in 1BMF) revealed that the distance between the –Cl group and the hydroxyl 5′-oxygen of ADP was only 1.61 Å away (Fig. 4A). However, in the final docked conformation, the distance was 2.44 Å (Fig. 4A). The analysis of the original ADP crystal structure showed that the distance was about 2.15 Å between the 5′-oxygen of ADP and the hydrogen at C8-

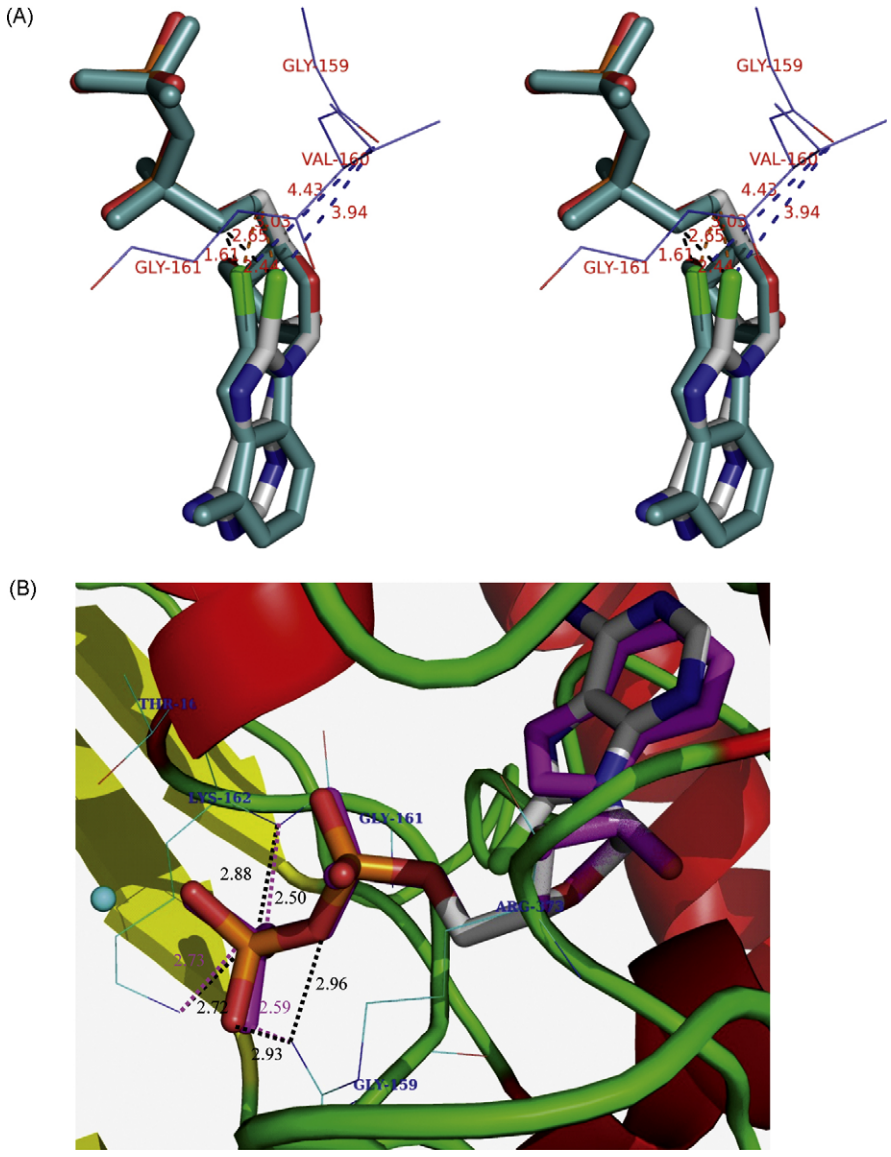

Fig. 4. Binding of 8-Cl-ADP to ATP synthase. (A) A stereo-view (wall-eyed) for the final docked (colored by atom types) and starting (light cyan) conformations of 8-Cl-ADP. Better geometry was obtained for the docked conformation. The lines represent key enzyme residues, and the –Cl group is shown in green. (B) Only one new hydrogen bond was observed between the binding pocket residues (α-Arg373) and 8-Cl-ADP β-phosphate group. ADP is shown in magenta and 8-Cl-ADP is colored by atom types. ATP synthase is displayed in secondary structure cartoon diagrams and some residues are displayed as color lines. Hydrogen bonds are represented by dashed lines (magenta for ADP and black for 8-Cl-ADP), and the cyan sphere represents Mg^{2+}.

position. Similarly we found that the distance between the 5′-carbon and the C8-position –Cl was 3.03 Å but in the starting conformation the distance was 2.65 Å (Fig. 4A). We also noticed that in ADP the distance between C8-position hydrogen and the carbon was 3.08 Å.

As part of our studies, hydrogen bonding interactions were also analyzed in the docked and crystal complexes. There was no tremendous difference of the hydrogen bonding patterns in the two structures, except that an additional hydrogen bond was formed between 8-Cl-ADP and the α-subunit Arg373 (Fig. 4B). No significant binding affinity change was observed based on our modeling prediction.

3.5. Inhibition of ATP accumulation in cells containing 8-Cl-ATP

To determine if intracellular 8-Cl-ATP can inhibit ATP synthase and hence the conversion of ADP to ATP, cells were treated with 8-Cl-Ado to accumulate 8-Cl-ATP. After washing the cells free of 8-Cl-Ado, they were incubated with [^{3}H]Ado and [^{3}H]AMP, ADP, and ATP were measured in previously untreated (control) or 8-Cl-Ado treated cells (Fig. 5A–C). Incubation of cells with 8-Cl-Ado resulted in about 450 μM 8-Cl-ATP with a 50% decline in ATP pool. Both in control and 8-Cl-Ado treated cells there was a rapid accumulation of [^{3}H]AMP, ADP, and ATP with ATP being the highest metabolite. In the 8-Cl-Ado pretreated cells, there was a significant increase in AMP formation ($p = 0.015$, Fig. 5A), no change in ADP accumulation ($p = 0.082$, Fig. 5B) and major decline in ATP ($p = 0.0009$, Fig. 5C). Cells treated with Ado alone accumulated about 220 μM of ATP at 0.5 h. This increased in a time-dependent fashion and reached to 720 μM at 3 h. Cells pretreated with 8-Cl-Ado showed a decline in ATP accumulation which was 160 μM at 0.5 h and 420 μM at 3 h (Fig. 5C). These data suggest that while similar levels of ADP were present in untreated or 8-Cl-Ado treated cells, 8-Cl-ATP accumulation was substantially reduced in 8-Cl-Ado pretreated cells suggesting inhibition of the ADP to ATP conversion step of ATP synthase by 8-Cl-ATP.

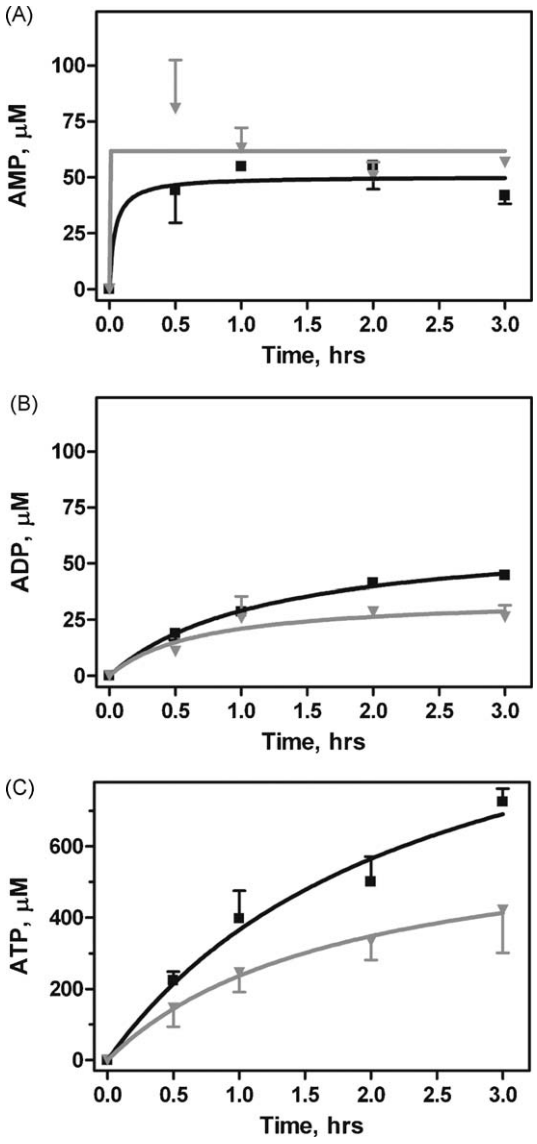

Fig. 5. Inhibition of phosphorylation of ADP to ATP in cells with intracellular 8-Cl-ATP. MM.1S cells were either untreated (black lines) or treated with 10 μM 8-Cl-Ado (gray lines) for 24 h, washed and then incubated with [^{3}H]Ado for indicated times. Accumulation of phosphorylated [^{3}H]Ado metabolites such as AMP (A), ADP (B), and ATP (C) was measured by HPLC as described in the Materials and Methods. Data points and error bars represent average of three experiments with S.D., and the results obtained were statistically significant ($p < 0.05$).

3.6. Molecular modeling with 8-Cl-ATP and ATP synthase

To further test inhibition of ATP synthase by 8-Cl-ATP, we did two sets of molecular modeling. First, 8-Cl-ATP was docked to the loose binding site ($\alpha_{tp}\beta_{tp}$) of the enzyme and second to the tight binding site ($\alpha_{dp}\beta_{dp}$). In the loose binding state of $\alpha_{tp}\beta_{tp}$ subunits, 8-Cl-ATP occupies very similar binding mode as ANP, which is usually used as an analogue of ATP to trap the enzyme in a structure closely related to the ATP-bound state because it cannot be hydrolyzed as ATP would be. As is shown in Fig. 6A, 8-Cl-ATP fits the binding pocket very well. Similar to the ADP binding observed, there is also a small pocket in this loose binding conformation to accommodate the chlorine atom (compared to the smaller hydrogen atom). In contrast, there was relatively large shift for the sugar ring of 8-Cl-ATP from the crystal structure of ANP sugar moiety (Fig. 6A). Hydrogen bond analysis (data not shown) demonstrated a few pattern changes of the interactions, but obviously the binding affinity did not change significantly.

We also docked 8-Cl-ATP into the tight binding site ($\alpha_{dp}\beta_{dp}$) based on the crystal structure of F_1 domain of 2CK3; the docked 8-Cl-ATP occupies a very similar position and orientation of ADP-BeF_3^-, the original inhibitor in 2CK3 (Fig. 6B). Three catalytically essential residues [23,24] α-Arg373, β-Arg189 and β-Lys162 are closer to the nucleotide in the docked complex than the ligand in the ADP-BeF_3^--F_1 structure, creating a tighter binding interface for the nucleotide (Fig. 6B).

Quantitatively, no large difference between the bindings of ADP/8-Cl-ADP and ATP/ANP/8-Cl-ATP to the enzyme was observed based on our modeling (Fig. 6C). AutoDock predicted both ADP and 8-Cl-ADP had about −10 kcal/mol docked energy (Fig. 6C), and for ATP/8-Cl-ATP, the binding was not as strong (below −7 kcal/mol) as ADP. With GOLD, similar results were obtained, although the fitness scores of 8-Cl-ADP/8-Cl-ATP were relatively lower than their corresponding natural substrates (Fig. 6C).

4. Discussion

F_1–F_O ATP synthase is a key manufacturing site of ATP. Given the critical role of ATP synthase, major efforts have been made to probe its protein structure and function. The availability of the structural information about ATP synthase F1 domain enabled us to conduct molecular docking studies of 8-Cl-Ado. Such methods have been widely used in drug discovery as well as in protein-ligand binding and interactions [35–40]. The structure of the F_1 unit has been studied by a variety of methods [23,41–44]. The first atomic resolution F_1 subunit crystal structure (1BMF) [23] was employed in our study since it is used frequently as a reference structure and believed to represent a conformation in the active catalytic cycle [23,24]. The crystal structures and ATPase reaction using F1 have been reported in detail because this portion of the enzyme could be isolated, is soluble, and functional in vitro, while the total ATP synthase requires proton motive force to run this enzymatic machinery as a rotary pump [45–47]. Due to this, ATP synthase requires either mitochondrial preparation, reconstitution in liposomes, and/or isolation from the cell surface, which makes biochemical studies challenging [48]. In the present investigation, we relied on molecular modeling as well as whole cell assays using 8-Cl-Ado, Ado, and pharmacological inhibitor of the enzyme, oligomycin.

4.1. 8-Cl-ADP as a substrate for ATP synthase

Due to the similarity between ADP and 8-Cl-ADP, we hypothesized that 8-Cl-ADP can bind to the ATP synthase tight binding site ($\alpha_{dp}\beta_{dp}$) of F_1 catalytic domain and act as an alternate substrate. Several lines of evidence suggest a possibility for this postulate. First, the ATP synthesis requires functional activity of complexes I–IV for complex V (ATP synthase) to be active. None of these first four complexes on the mitochondrial membrane were affected by 8-Cl-Ado (Fig. 1), suggesting that the last complex may be the target for this inhibition. Second, as observed for ATP formation from ADP, the accumulation of 8-Cl-ATP from 8-Cl-ADP was decreased by oligomycin, an inhibitor of F_O subunit of ATP synthase (Fig. 2). Third, decrease in 8-Cl-ATP accumulation is not due to decrease in ATP (a phosphate donor) as ara-CTP accumulation was not inhibited by oligomycin treatment. Fourth, 8-Cl-cAMP which serves as a prodrug for 8-Cl-Ado [6] also showed a decline in 8-Cl-ATP formation after oligomycin treatment. Finally, as detailed below, molecular modeling suggests that the chlorinated ADP binds well at the substrate binding site of the ATP synthase.

(A)

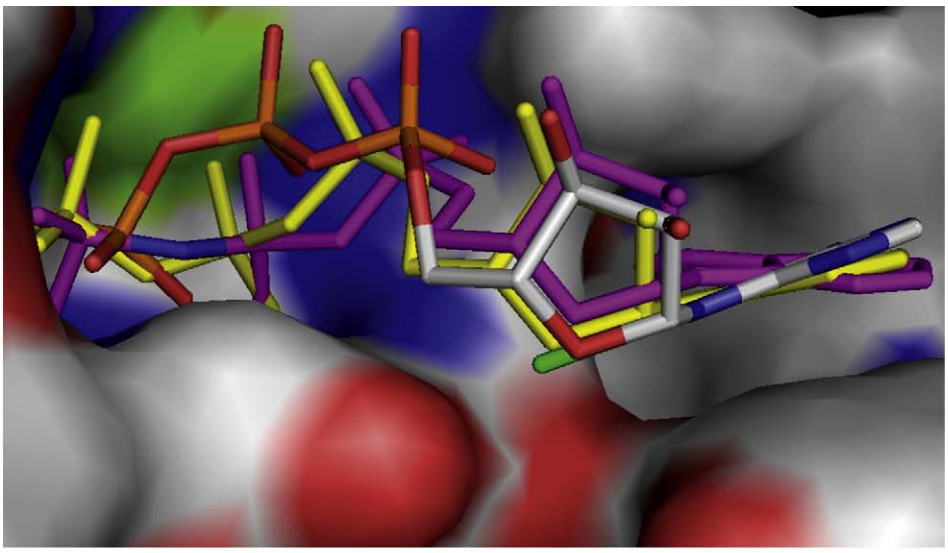

(B)

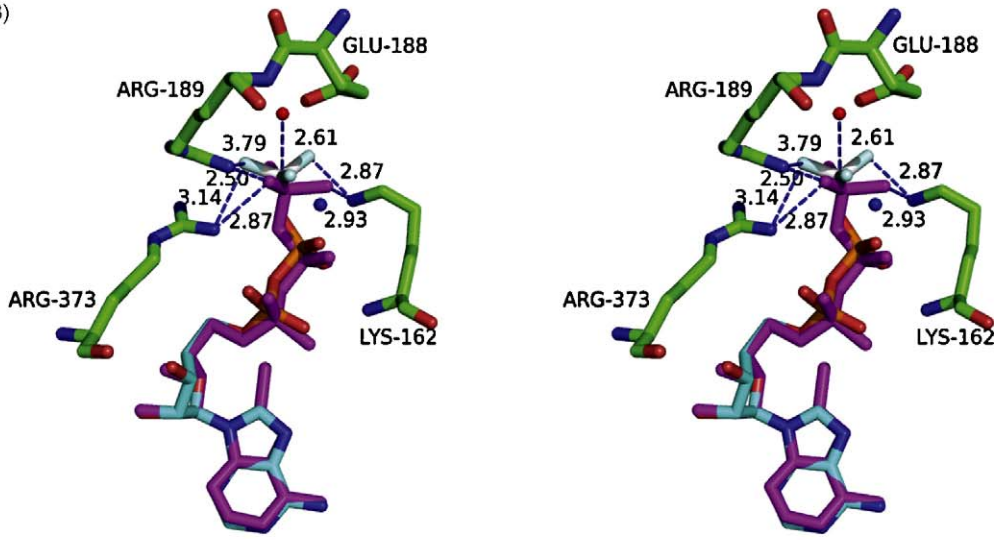

(C)

Ligands	Docked Energy (AutoDock)	Fitness (GOLD)	Docking Site
ADP	-11.08	65.36	1BMF $\alpha_{dp}\beta_{dp}$
8-Cl-ADP	-10.78	49.27	1BMF $\alpha_{dp}\beta_{dp}$
ATP	-6.88	92.31	1BMF $\alpha_{tp}\beta_{tp}$
8-Cl-ATP	-5.45	74.37	1BMF $\alpha_{tp}\beta_{tp}$
ANP	-9.26	91.38	1BMF $\alpha_{tp}\beta_{tp}$
8-Cl-ATP	-11.65	76.45	2CK3 $\alpha_{dp}\beta_{dp}$
ADP-BeF_3^-	-10.44	70.33	2CK3 $\alpha_{dp}\beta_{dp}$

Fig. 6. Surface analysis and binding of the product 8-Cl-ATP to ATP synthase. (A) The surface analysis of the $\alpha_{tp}\beta_{tp}$ subunit binding pocket, which reveals a concave region to accommodate the –Cl group (green). The green surface represents Mg^{2+}, and the color coded surface based on atom types is for the receptor binding pocket. Atom type-based color coded stick represents docked 8-Cl-ATP. Docked ATP is shown in yellow sticks and magenta represents the crystal ANP. (B) Wall-eyed stereo representation provides a comparison of the catalytic sites in the docked 8-Cl-ATP-F_1 and crystal ADP-BeF_3^--F_1 structures. In the 8-Cl-ATP-F_1 structure, γ-phosphate is bound in a similar position to those three fluorides mimicking ATP binding in the active enzyme. The catalytically essential α-Arg373, β-Arg189 and β-Lys162 are closer to the nucleotide in the docked complex than those in the ADP-BeF_3^--F_1 structure, creating a tighter binding interface for the nucleotide. (C) Docking results from AutoDock and GOLD. The metabolites of Ado and halogenated analogues were docked into the diphosphate ($\alpha_{dp}\beta_{dp}$) and triphosphate ($\alpha_{tp}\beta_{tp}$) binding sites of ATP synthase structure.

4.2. Molecular modeling with 8-Cl-ADP and ATP synthase

Molecular docking results on 8-Cl-ADP was very similar to ADP except a small shift of the whole structure and an obvious protrusion of the –Cl group towards a small pocket formed by residues Ala158, Gly159, Gly161 and Val164, all of which have relatively short side chains (Fig. 6C). The protrusion was both due to the large –Cl group as well as the 22.60° tilting of the purine ring compared to ADP crystal structure. The modeling indicated likely conformational changes in the 8-Cl-ADP structure to accommodate the C8-chlorine atom. In the starting 8-Cl-ADP conformation the distance between the chlorine atom and the 5′-oxygen of ADP was only about 1.61 Å (Fig. 4A), which would most likely cause clashes. In the final docked conformation the distance increased to 2.44 Å, which is closer to the same distance in the original ADP crystal structure (2.15 Å). Similarly, the distance between the 5′-carbon atom and the C8-position chlorine (3.03 Å) became more comparable with that of ADP (3.08 Å), indicating that the docked conformation was optimized by shifting the adenine ring to reduced the geometric deficiency caused by C8-substitution. In addition, the chlorine and oxygen interactions become evident in the docked structure. The distance between the Gly159 carbonyl oxygen and the chlorine is 3.94 Å compared to 4.43 Å in the starting conformation (Fig. 4A), and the angle of the C–Cl–O is about 150°. According to a recent study [49], the interaction between carbon-bonded halogens (Cl, Br and I) and electronegative atoms (O, N and S) were not marginal and the attractive natures of these types of interactions were due to strong electrostatic effects. Thus the C–Cl–O interaction here most probably further stabilized the binding of 8-Cl-ADP to ATP synthase.

Although the replacement of C8-hydrogen with chlorine produced a small shift of the binding conformation, it did not dramatically influence the hydrogen bonding interactions. In particular, with residue Lys162 the distance between the β-phosphate and ε-amino group only changed about 0.01 Å (Fig. 4B). There is less than 0.4 Å change of the distance between the oxygen atoms of 8-Cl-ADP β-phosphate group and Lys162/Arg373, placing the interactions within hydrogen bonding distance. Other than those, the diphosphate group bridging oxygen (–P–O–P–) is about 2.93 Å away from one of the guanidinium nitrogen atoms of Arg373, which is predicted to be involved in hydrogen bonding interactions. Interestingly, perhaps compensated by the distance change of the other two hydrogen bonds, this additional hydrogen bond does not lead to large binding affinity change (Figs. 4B and 6C), indicating that ADP and 8-Cl-ADP could be competitively bound to ATP synthase F1 domain.

4.3. 8-Cl-ATP as an inhibitor of ATP synthase

Based on the similarity between ATP and 8-Cl-ATP, we hypothesized that 8-Cl-ATP can bind to the tight binding site ($\alpha_{dp}\beta_{dp}$) and loose binding conformation ($\alpha_{tp}\beta_{tp}$), therefore acting as an inhibitor for the function of the enzyme. Cellular accumulation of ATP was affected in cells that were loaded with 8-Cl-ATP (Fig. 5C) without much effect on AMP and ADP formation. These whole cell data suggest that 8-Cl-Ado metabolites may decrease conversion of intracellular ADP to ATP.

4.4. Molecular modeling with 8-Cl-ATP and ATP synthase

Docking of 8-Cl-ATP to ATP synthase demonstrated that 8-Cl-ATP occupied a very similar binding mode as ANP, with the exception of a relatively large shift in the sugar ring of 8-Cl-ATP. This conformational deviation did not generate geometrical clashes, and thus 8-Cl-ATP fit in the pocket complementarily (Fig. 6A). The large shift might be the overall effect of the replacement of C8-position hydrogen with chlorine as well as the substitution of nitrogen in –P–N–P– with oxygen. Analysis of the hydrogen bonding demonstrated a few changes (Fig. 6C), however, the binding affinity did not change dramatically suggesting that like ANP, 8-Cl-ATP may inhibit ATP synthase.

Recently Walker and co-workers reported that F_1-ATPase was inhibited by ADP-BeF_3^-, which is also an ATP analogue [24]. Interestingly, when 8-Cl-ATP was docked into the tight binding site ($\alpha_{dp}\beta_{dp}$) of 2CK3, it was observed to form tighter interactions with the enzyme. ATP synthase was inhibited by its co-crystallized ligand ADP-BeF_3^- via mimicking ATP structure, and residue α-Arg373 could sense the presence/absence of the γ-phosphate of the ligand [24]. The docked 8-Cl-ATP occupies very similar position and orientation of ADP-BeF_3^- (Fig. 6B). However, 8-Cl-ATP seems closer to the catalytically essential residue [23,24] (α-Arg373, β-Arg189, β-Lys162 and β-Glu188) in the docked complex than ADP-BeF_3^- in the crystal structure, and thus may lead to strong interactions with ATP synthase (Fig. 6B). These observations provide an explanation why the endogenous ATP was dramatically decreased with the increase of 8-Cl-ATP.

Based on our calculations, the binding affinities of ADP/ATP and 8-Cl-ADP/8-Cl-ATP to the enzyme were similar (Fig. 6C). This result suggested that 8-Cl-ADP and 8-Cl-ATP might be the competitors of ADP and ATP, respectively. This supports our experimental findings that the endogenous ATP pool usually declined 40–50% several hours after 8-Cl-Ado was added to the system. With results from GOLD, similar conclusions were obtained, although the fitness scores of 8-Cl-ADP/8-Cl-ATP were lower than their correspondent natural substrates, which can be due to the different implementation of the two docking packages.

Additionally as expected, the calculated binding energy is much higher when 8-Cl-ATP was docked into the tight binding site of ATP synthase F1 domain, comparable to the original bound ligand ADP-BeF_3^-, which was found to inhibit the enzyme. Previously identified inactivators of F1 ATPase include covalent inhibitors such as 4-Cl-7-nitrobenzofurazan [50] and dicyclohexylcarbodiimide [51,52], and non-covalent inhibitors such as azide [53], IF1 [54], efrapeptin [55], polyphenolic phytochemicals [56] including resveratrol [57]. The efrapeptin prevents the open-form of beta subunit to close; preventing substrate binding to the catalytic site [55], whereas aurovertin B, appears to prevent closure of the catalytic site [58]. Oligomycin, another antibiotic, affects the F_O, membrane intrinsic subunit of the enzyme. In contrast to these inactivators, 8-Cl-Ado appears to serve as both alternate substrate (as diphosphate) and inhibitor (as triphosphate), making it a unique inhibitor of the enzyme. It is interesting to note that treatment with a related analogue, N^6-furfuryladenosine, also results in marked ATP depletion in various cancer cell lines, however it is unknown at the present time whether its action is via ATP synthase inhibition [59,60].

Our studies presented here demonstrate that predictions from computational molecular modeling can be further validated by experimental methods in cellular systems, which provide a unique mechanism of action for 8-Cl-Ado. Our data shed light on the complex mechanism by which 8-Cl-ATP accumulation results in decline in cellular bioenergy. Cancer cells rely highly on cellular bioenergy metabolism and 8-Cl-Ado is in the clinic as an anticancer agent, therefore, our current results provide insight into the mechanism of action for this novel ATP analogue.

Acknowledgements

This work is supported in part by grant CA85915 from the National Cancer Institute, Department of Health and Human Services, a Translational Research Award from Leukemia and Lymphoma Society of America, and a University of Texas M. D. Anderson Cancer Center Start-up Fund to SZ.

Appendix A. Supplementary data

Supplementary data associated with this article can be found, in the online version, at doi:10.1016/j.bcp.2009.05.019.

References

[1] Plunkett W, Gandhi V. Purine and pyrimidine nucleoside analogs. Cancer Chemother Biol Response Modif 2001;19:21–45.
[2] Bonate PL, Arthaud L, Cantrell Jr WR, Stephenson K, Secrist 3rd JA, Weitman S. Discovery and development of clofarabine: a nucleoside analogue for treating cancer. Nat Rev Drug Discov 2006;5:855–63.
[3] Gandhi V, Kilpatrick JM, Plunkett W, Ayres M, Harman L, Du M, et al. A proof-of-principle pharmacokinetic, pharmacodynamic, and clinical study with purine nucleoside phosphorylase inhibitor immucillin-H (BCX-1777, forodesine). Blood 2005;106:4253–60.
[4] Ho AD, Hensel M. Pentostatin for the treatment of indolent lymphoproliferative disorders. Semin Hematol 2006;43:S2–10.
[5] Kay NE. Purine analogue-based chemotherapy regimens for patients with previously untreated B-chronic lymphocytic leukemia. Semin Hematol 2006;43:S50–4.
[6] Gandhi V, Ayres M, Halgren RG, Krett NL, Newman RA, Rosen ST. 8-chloro-cAMP and 8-chloro-adenosine act by the same mechanism in multiple myeloma cells. Cancer Res 2001;61:5474–9.
[7] Stellrecht CM, Rodriguez Jr CO, Ayres M, Gandhi V. RNA-directed actions of 8-chloro-adenosine in multiple myeloma cells. Cancer Res 2003;63:7968–74.
[8] Chen LS, Sheppard TL. Chain termination and inhibition of *Saccharomyces cerevisiae* poly(A) polymerase by C-8-modified ATP analogs. J Biol Chem 2004;279:40405–11.
[9] Bennett Jr LL, Allan PW, Chang CH. Phosphorylation of "tricyclic nucleoside" by adenosine kinases from L1210 cells and HEp-2 cells. Biochem Pharmacol 1983;32:2601–2.
[10] Balakrishnan K, Stellrecht CM, Genini D, Ayres M, Wierda WG, Keating MJ, et al. Cell death of bioenergetically compromised and transcriptionally challenged CLL lymphocytes by chlorinated ATP. Blood 2005;105:4455–62.
[11] Boyer PD. What makes ATP synthase spin? Nature 1999;402:247–9.
[12] Capaldi RA, Aggeler R. Mechanism of the F(1)F(0)-type ATP synthase, a biological rotary motor. Trends Biochem Sci 2002;27:154–60.
[13] Leyva JA, Bianchet MA, Amzel LM. Understanding ATP synthesis: structure and mechanism of the F1-ATPase (Review). Mol Membr Biol 2003;20:27–33.
[14] Oster G, Wang H. ATP synthase: two motors, two fuels. Structure 1999;7:R67–72.
[15] Stock D, Gibbons C, Arechaga I, Leslie AG, Walker JE. The rotary mechanism of ATP synthase. Curr Opin Struct Biol 2000;10:672–9.
[16] Hong S, Pedersen PL. ATP synthase and the actions of inhibitors utilized to study its roles in human health, disease, and other scientific areas. Microbiol Mol Biol Rev 2008;72:590–641.
[17] Chang SY, Park SG, Kim S, Kang CY. Interaction of the C-terminal domain of p43 and the alpha subunit of ATP synthase, Its functional implication in endothelial cell proliferation. J Biol Chem 2002;277:8388–94.
[18] Scotet E, Martinez LO, Grant E, Barbaras R, Jeno P, Guiraud M, et al. Tumor recognition following Vgamma9Vdelta2 T cell receptor interactions with a surface F1-ATPase-related structure and apolipoprotein A-I. Immunity 2005;22:71–80.
[19] Moser TL, Kenan DJ, Ashley TA, Roy JA, Goodman MD, Misra UK, et al. Endothelial cell surface F1-F0 ATP synthase is active in ATP synthesis and is inhibited by angiostatin. Proc Natl Acad Sci USA 2001;98:6656–61.
[20] Huang TC, Chang HY, Hsu CH, Kuo WH, Chang KJ, Juan HF. Targeting therapy for breast carcinoma by ATP synthase inhibitor aurovertin B. J Proteome Res 2008;7:1433–44.
[21] Chi SL, Wahl ML, Mowery YM, Shan S, Mukhopadhyay S, Hilderbrand SC, et al. Angiostatin-like activity of a monoclonal antibody to the catalytic subunit of F1F0 ATP synthase. Cancer Res 2007;67:4716–24.
[22] Wang J, Han Y, Liang J, Cheng X, Yan L, Wang Y, et al. Effect of a novel inhibitory mAb against beta-subunit of F1F0 ATPase on HCC. Cancer Biol Ther 2008;7.
[23] Abrahams JP, Leslie AG, Lutter R, Walker JE. Structure at 2.8 A resolution of F1-ATPase from bovine heart mitochondria. Nature 1994;370:621–8.
[24] Kagawa R, Montgomery MG, Braig K, Leslie AG, Walker JE. The structure of bovine F1-ATPase inhibited by ADP and beryllium fluoride. EMBO J 2004;23:2734–44.
[25] Goldman-Leikin RE, Salwen HR, Herst CV, Variakojis D, Bian ML, Le Beau MM, et al. Characterization of a novel myeloma cell line MM.1. J Lab Clin Med 1989;113:335–45.
[26] Krett NL, Zell JL, Halgren RG, Pillay S, Traynor AE, Rosen ST. Cyclic adenosine-3′,5′-monophosphate-mediated cytotoxicity in steroid sensitive and resistant myeloma. Clin Cancer Res 1997;3:1781–7.
[27] Hail Jr N, Youssef EM, Lotan R. Evidence supporting a role for mitochondrial respiration in apoptosis induction by the synthetic retinoid CD437. Cancer Res 2001;61:6698–702.
[28] Pelicano H, Feng L, Zhou Y, Carew JS, Hileman EO, Plunkett W, et al. Inhibition of mitochondrial respiration: a novel strategy to enhance drug-induced apoptosis in human leukemia cells by a reactive oxygen species-mediated mechanism. J Biol Chem 2003;278:37832–9.
[29] Rodriguez Jr CO, Plunkett W, Paff MT, Du M, Nowak B, Ramakrishna P, et al. High-performance liquid chromatography method for the determination and quantitation of arabinosylguanine triphosphate and fludarabine triphosphate in human cells. J Chromatogr B Biomed Sci Appl 2000;745:421–30.
[30] Berman HM, Westbrook J, Feng Z, Gilliland G, Bhat TN, Weissig H, et al. The Protein Data Bank. Nucleic Acids Res 2000;28:235–42.
[31] GOLD. Cambridge, UK: CCDC; 2007.
[32] AutoDock. La Jolla, CA: Scripps Research Institute; 1999.
[33] MOE. Montréal, Québec, Canada: Chemical Computing Group; 2006.
[34] PyMol. Palo Alto, CA: DeLano Scientific LLC; 2007.
[35] Gschwend DA, Good AC, Kuntz ID. Molecular docking towards drug discovery. J Mol Recognit 1996;9:175–86.
[36] Oloff S, Zhang S, Sukumar N, Breneman C, Tropsha A. Chemometric analysis of ligand receptor complementarity: identifying Complementary Ligands Based on Receptor Information (CoLiBRI). J Chem Inf Model 2006;46:844–51.
[37] Taylor RD, Jewsbury PJ, Essex JW. A review of protein-small molecule docking methods. J Comput Aided Mol Des 2002;16:151–66.
[38] Zhang S, Du-Cuny L. Development and evaluation of a new statistical model for structure-based high-throughput virtual screening. Int J Bioinf Res Appl 2009;5:269–79.
[39] Zhang S, Golbraikh A, Tropsha A. Development of quantitative structure-binding affinity relationship models based on novel geometrical chemical descriptors of the protein-ligand interfaces. J Med Chem 2006;49:2713–24.
[40] Zhang S, Ying WS, Siahaan TJ, Jois SDS. Solution structure of a peptide derived from the beta subunit of LFA-1. Peptides 2003;24:827–35.
[41] Boekema EJ, Berden JA, van Heel MG. Structure of mitochondrial F1-ATPase studied by electron microscopy and image processing. Biochim Biophys Acta 1986;851:353–60.
[42] Wilkens S, Borchardt D, Weber J, Senior AE. Structural characterization of the interaction of the delta and alpha subunits of the *Escherichia coli* F1F0-ATP synthase by NMR spectroscopy. Biochemistry 2005;44:11786–94.
[43] Abrahams JP, Lutter R, Todd RJ, van Raaij MJ, Leslie AG, Walker JE. Inherent asymmetry of the structure of F1-ATPase from bovine heart mitochondria at 6.5 A resolution. EMBO J 1993;12:1775–80.
[44] Lutter R, Abrahams JP, van Raaij MJ, Todd RJ, Lundqvist T, Buchanan SK, et al. Crystallization of F1-ATPase from bovine heart mitochondria. J Mol Biol 1993;229:787–90.
[45] Kinosita Jr K, Yasuda R, Noji H, Ishiwata S, Yoshida M. F1-ATPase: a rotary motor made of a single molecule. Cell 1998;93:21–4.
[46] Noji H, Yasuda R, Yoshida M, Kinosita Jr K. Direct observation of the rotation of F1-ATPase. Nature 1997;386:299–302.
[47] Senior AE, Weber J. Happy motoring with ATP synthase. Nat Struct Mol Biol 2004;11:110–2.
[48] Senior AE, Nadanaciva S, Weber J. The molecular mechanism of ATP synthesis by F1F0-ATP synthase. Biochim Biophys Acta 2002;1553:188–211.
[49] Lommerse JPM, Stone AJ, Taylor R, Allen FH. The nature and geometry of intermolecular interactions between halogens and oxygen or nitrogen. J Am Chem Soc 1996;118:3108–16.
[50] Orriss GL, Leslie AG, Braig K, Walker JE. Bovine F1-ATPase covalently inhibited with 4-chloro-7-nitrobenzofurazan: the structure provides further support for a rotary catalytic mechanism. Structure 1998;6:831–7.
[51] Gledhill JR, Walker JE. Inhibitors of the catalytic domain of mitochondrial ATP synthase. Biochem Soc Trans 2006;34:989–92.
[52] Yoshida M, Allison WS. The ATPase activity of the alpha 3 beta 3 complex of the F1-ATPase of the thermophilic bacterium PS3 is inactivated on modification of tyrosine 307 in a single beta subunit by 7-chloro-4-nitrobenzofurazan. J Biol Chem 1990;265:2483–7.
[53] Bowler MW, Montgomery MG, Leslie AG, Walker JE. How azide inhibits ATP hydrolysis by the F-ATPases. Proc Natl Acad Sci USA 2006;103:8646–9.
[54] Gledhill JR, Montgomery MG, Leslie AG, Walker JE. How the regulatory protein, IF(1), inhibits F(1)-ATPase from bovine mitochondria. Proc Natl Acad Sci USA 2007;104:15671–6.
[55] Abrahams JP, Buchanan SK, Van Raaij MJ, Fearnley IM, Leslie AG, Walker JE. The structure of bovine F1-ATPase complexed with the peptide antibiotic efrapeptin. Proc Natl Acad Sci USA 1996;93:9420–4.
[56] Zheng J, Ramirez VD. Inhibition of mitochondrial proton F0F1-ATPase/ATP synthase by polyphenolic phytochemicals. Br J Pharmacol 2000;130:1115–23.
[57] Gledhill JR, Montgomery MG, Leslie AG, Walker JE. Mechanism of inhibition of bovine F1-ATPase by resveratrol and related polyphenols. Proc Natl Acad Sci USA 2007;104:13632–7.
[58] van Raaij MJ, Abrahams JP, Leslie AG, Walker JE. The structure of bovine F1-ATPase complexed with the antibiotic inhibitor aurovertin B. Proc Natl Acad Sci USA 1996;93:6913–7.
[59] Tiedemann RE, Mao X, Shi CX, Zhu YX, Palmer SE, Sebag M, et al. Identification of kinetin riboside as a repressor of CCND1 and CCND2 with preclinical antimyeloma activity. J Clin Invest 2008;118:1750–64.
[60] Cabello CM, Bair 3rd WB, Ley S, Lamore SD, Azimian S, Wondrak GT. The experimental chemotherapeutic N(6)-furfuryladenosine (kinetin-riboside) induces rapid ATP depletion, genotoxic stress, and CDKN1A(p21) upregulation in human cancer cell lines. Biochem Pharmacol 2009;77:1125–38.